ACS OMEGA

http://pubs.acs.org/journal/acsodf

Article

Modified Flowing Material Balance Equation for Shale Gas Reservoirs

Long Yang, Yizhong Zhang,* Maolin Zhang, Yong Liu, Zhenqiang Bai, and Bin Ju

Cite This: *ACS Omega* 2022, 7, 20927−20944

Read Online

ACCESS | Metrics & More | Article Recommendations

ABSTRACT: To determine original gas-in-place, this study establishes a flowing material balance equation based on the improved material balance equation for shale gas reservoirs. The method considers the free gas in the matrix and fracture, the dissolved gas in kerogen, and the pore volume occupied by adsorbed phase simultaneously, overcoming the problem of incomplete consideration in the earlier models. It also integrates the material balance method with the flowing material balance method to obtain the average formation pressure, eliminating the problem with the previous method where shutting down of wells was needed to monitor the formation pressure. The volume of the adsorbed gas on the ground is converted into volume of the adsorbed phase in the formation using the volume conservation method to characterize the pore volume occupied by the adsorbed phase, which solves the problem of the previous model that the adsorbed phase was neglected in the pore volume. The model proposed in this study is applied to the Fuling Shale Gas Field in southwest China and compared with other flowing material balance equations, and the results show that the single-well control area calculated by the model proposed in this study is closer to the real value, indicating that the calculations in this study are more accurate. Furthermore, the calculations show that the dissolved gas takes up a large fraction of the total reserves and cannot be ignored. The sensitivity analyses of critical parameters demonstrate that (a) the greater the porosity of the fracture, the greater the free gas storage; (b) the values of Langmuir volume and TOC can significantly affect the results of the reservoir calculation; and (c) the adsorbed phase occupies a smaller pore volume when the Langmuir volume is smaller, the Langmuir pressure is higher, or the adsorbed phase density is higher. The findings of this study can provide better understanding of the necessity to take into account the dissolved gas in the kerogen, the pore volume occupied by the adsorbed phase, and the fracture porosity when evaluating reserves. The method could be applied to the calculation of pressure, recovery of free gas phase and adsorbed phase, original gas-in-place, and production predictions, which could help for better guidance of reserve potential estimations and development strategies of shale gas reservoirs.

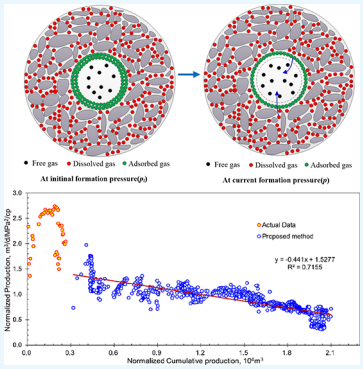

1. INTRODUCTION

With the increase of the world energy demand, unconventional gas resources have attracted attention worldwide.[1−3] Compared to conventional gas reservoirs, shale gas has its characteristics. First, shale has extremely low permeability and high heterogeneity. Re-equilibrium of the fluids will be time-consuming for the build-up well tests, and a material balance equation based on the static and dynamic reservoir parameters could be an expected method to characterize the shale gas reservoirs. Second, in terms of storage mechanism, gas mainly exists in adsorbed, free, and dissolved states in the shale.[4−7] Thus, the calculation methods for conventional reserves may not be applied to shale gas.[8,9] Previous scholars studied the calculation of the original gas-in-place (OGIP) of shale gas, and factors such as free gas, adsorbed gas, dissolved gas, rock stress sensitivity, and irreducible water expansion have been taken into consideration, making their models closer to the real gas reservoir.[10−13] However, there are still important factors that have not been considered, including the influence of free gas in the fracture and the volume of the adsorbed phase in the pore space. The above factors should be considered comprehensively to calculate the OGIP of shale gas accurately.

The material balance equation of coalbed methane considering the effects of water influx and adsorbed gas was first proposed by King.[10] The OGIP could be calculated using the slope and intercept of p/Z^* (ratio of pressure and modified Z-factor) versus G_p (cumulative gas production). Based on King's work, Ahmed et al.[11] established the material balance equation of coalbed methane considering free gas, adsorbed gas, irreducible water expansion, and stress sensitivity, and they applied it to solve the average formation pressure. Moghadam et al.[14] redefined the Z-factor according to the principle of volume

Received: March 18, 2022
Accepted: May 19, 2022
Published: June 7, 2022

https://doi.org/10.1021/acsomega.2c01662
ACS Omega 2022, 7, 20927−20944

conservation and extended the material balance equation to all gas reservoirs and used the bottom hole pressure (BHP) to calculate OGIP when in a pseudo-steady flow. Mattar and McNeil[15] proposed the flowing material balance method, which used BHP instead of average formation pressure to calculate reserves. Anderson et al.[16] proposed material balance pseudo-time and extended this method from constant BHP or constant production rate to changed production rates and changed production pressures. Considering the adsorbed gas, the flowing material balance equation of the coalbed methane reservoir was established by Clarkson et al.[17]

However, according to Ambrose et al.,[18] the volume of adsorbed phase could not be ignored, and the volume of the adsorbed phase needs to be subtracted from the void space measured by porosity measurement (Figure 1). The previously

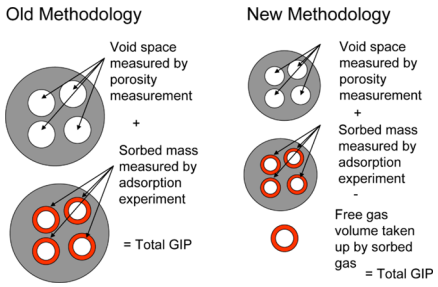

Figure 1. Comparison of the old and new methodologies in predicting shale gas-in-place. Reprinted (adapted or reprinted in part) with permission from ref 18.

mentioned material balance equations did not consider the pore volume occupied by the adsorbed phase and overestimated the volume occupied by the free gas, resulting in inaccurate calculations of total reserves. In addition, shale gas has the characteristics of low permeability and high heterogeneity, necessitating hydraulic fracturing to achieve industrial production.[19−21] The compressibility of fracture is much higher than that of the matrix, and the porosity of fracture and matrix varies with pressure.[22−25] Thus, the influence of fracture should be considered in the improved material balance equations. As free gas is produced and formation pressure drops, the adsorbed gas begins to desorb and dissolved gas begins to diffuse, supplying formation energy. Thus, the mechanism of adsorbed gas desorption and dissolved gas diffusion should be considered in the new method.

The influences of adsorbed phase volume, dissolved gas, and free gas on fracture were not fully included in prior approaches for computing reserves of shale gas reservoirs, resulting in discrepancies in reserve calculation results.[26−30] The adsorption model and multiscale gas fluid flow are considered to describe the volume change of gas adsorption/desorption and gas dissolution. By rebuilding the pore volume model, the volume change of gas in kerogen, matrix, and fractures, the volume changes due to stress sensitivity and irreducible water expansion, and volume change due to adsorbed gas desorption are considered. Thus, based on the previous studies, this study integrates various factors (adsorbed phase occupying pore volume, dissolved gas in kerogen, free gas in both fracture and matrix, stress sensitivity, irreducible water expansion, and adsorbed gas) to establish a new material balance equation for shale gas reservoirs, addressing issues such as the inadequacy of prior methods to account for free gas in fractures, pore volume occupied by adsorbed gas, and the challenging problem of obtaining formation pressure. The general sketch diagram of the method used in this study is shown in Figure 2.

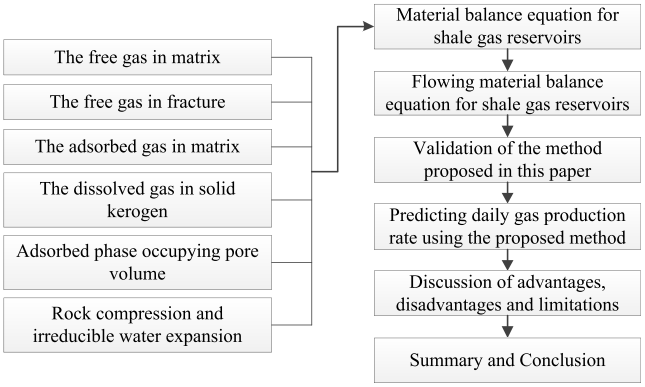

Figure 2. General sketch diagram of the study problem.

In this study, the shale gas reservoir material balance method considering multiple factors and the flowing material balance method is established in Section 2. The accuracy of the method proposed in this study is verified in Section 3.1. The gas rate is predicted in Section 3.2 using the method proposed in this study. The sensitivity analysis of critical parameters is detailed in Section 3.3. The advantages, disadvantages, and limitations of the proposed method are given in Section 3.4. The summary and conclusions of this study are given in Section 4.

2. METHODOLOGY

This study has the following assumptions when the material balance equations are established for shale gas reservoirs: (1) shale gas reservoirs are isothermal; (2) matrix and fractures systems have different irreducible water saturation; (3) water influx and water production are not considered and only free gas flows in the fracture are considered;[31] (4) adsorbed gas is adsorbed on the inner surface of the matrix; and (5) shale gas reservoirs have double porosity (matrix, fractures) and single permeability (fractures).

The shale gas mainly contains adsorbed, free, and dissolved gas stored in the matrix and fractures. The OGIP contains four parts: the adsorbed gas in the matrix, the free gas in the matrix, the free gas in the fractures, and the dissolved gas in the kerogen.

The free gas porosity in the matrix (as shown in Appendix A) is:

$$\phi_m = \phi_{mt}(1 - s_{mwc}) - \frac{\rho_b V_E(p_i)\rho_{sc}}{\rho_s} \quad (1)$$

Considering the Langmuir isotherm adsorption model,[32] the relationship is as follows:

$$V_E(p) = \frac{V_L p}{p_L + p} \quad (2)$$

The volume of the matrix (as shown in Appendix A) is:

$$V_m = \frac{G_m B_{gi}}{\phi_m} \quad (3)$$

The fracture pore volume (V_f) at the initial formation pressure (as shown in Appendix A) can be calculated as follows:

https://doi.org/10.1021/acsomega.2c01662
ACS Omega 2022, 7, 20927−20944

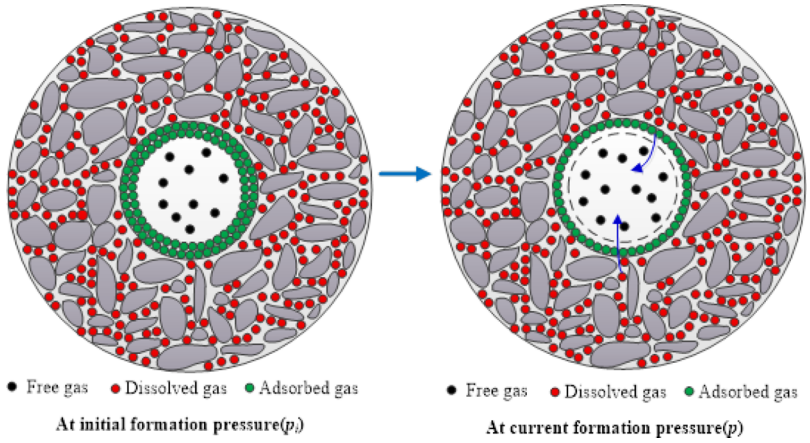

Figure 3. Schematic diagram of the change in the volume of the adsorbed phase as the pressure decreases.

$$V_f = \frac{G_m B_{gi} \phi_f}{\phi_m} \tag{4}$$

The free gas reserves in the fractures (G_f) at the initial formation pressure (p_i) can be calculated as follows:

$$G_f = \frac{V_f(1 - s_{fwc})}{B_{gi}} = G_m \frac{(1 - s_{fwc})\phi_f}{\phi_m} \tag{5}$$

The free gas reserves in the fractures and matrix (G_{free}) at the initial formation pressure (p_i) can be calculated as follows:

$$G_{free} = G_m \left(1 + \frac{(1 - s_{fwc})\phi_f}{\phi_m}\right) \tag{6}$$

The reserves of adsorbed gas (G_a) at the initial formation pressure (p_i) can be expressed as follows:

$$G_a = \frac{G_m B_{gi} \rho_b}{\phi_m} V_E(p_i) \tag{7}$$

The dissolved gas reserves (G_d) in kerogen at the initial formation pressure (p_i) can be expressed as follows:

$$G_d = c(p_i) \frac{G_m B_{gi} V_{diff}}{\phi_m} \tag{8}$$

Mehrotra and Svrcek[33] gave the solubility expression as follows:

$$c(p) = 1.0732 \times \left(b_1 + b_2 p + b_3 \frac{p}{T} + b_4 \left(\frac{p}{T}\right)^2\right) \tag{9}$$

$$V_{diff} = \frac{TOC \times \rho_b}{100 \rho_{ko}} - \phi_a - \phi_{org} \tag{10}$$

The volume change of the adsorbed phase (as shown in Figure 3) can be calculated as follows:

$$\Delta V_a = \frac{G_m B_{gi} \rho_b \rho_{sc}}{\phi_m \rho_s} (V_E(p_i) - V_E(p)) \tag{11}$$

The volume of stress sensitivity and irreducible water expansion in the matrix can be calculated as:

$$\Delta V_{cm} = \frac{G_m B_{gi} \phi_{mt}}{\phi_m} [(1 - e^{-c_m(p_i - p)}) + s_{mwc}(e^{c_w(p_i - p)} - 1)] \tag{12}$$

Considering $e^x \approx 1 + x$, eq 12 can be expressed as:

$$\Delta V_{cm} = \frac{G_m B_{gi} \phi_{mt}}{\phi_m} (c_m + c_w s_{mwc})(p_i - p) \tag{13}$$

The volume of rock stress sensitivity and irreducible water expansion in the fractures can be calculated as:

$$\Delta V_{cf} = \frac{G_m B_{gi} \phi_f}{\phi_m} [(1 - e^{-c_f(p_i - p)}) + s_{fwc}(e^{c_w(p_i - p)} - 1)] \tag{14}$$

Considering $e^x \approx 1 + x$, eq 14 can be expressed as:

$$\Delta V_{cf} = \frac{G_m B_{gi} \phi_f}{\phi_m} (c_f + c_w s_{fwc})(p_i - p) \tag{15}$$

With the exploitation of shale gas, the pore volume of the reserves is affected by multiple effects of the volume change of the adsorbed phase, the stress sensitivity of the rock, and the expansion of irreducible water. Therefore, the change volume of the pore is expressed as follows:

$$\begin{aligned} \Delta V &= \Delta V_a - \Delta V_{cm} - \Delta V_{cf} \\ &= \frac{G_m B_{gi} \rho_b \rho_{sc}}{\phi_m \rho_s} (V_E(p_i) - V_E(p)) - \frac{G_m B_{gi} \phi_{mt}}{\phi_m} \\ &\quad (c_m + c_w s_{mwc})(p_i - p) - \frac{G_m B_{gi} \phi_f}{\phi_m} (c_f + c_w s_{fwc}) \\ &\quad (p_i - p) \end{aligned} \tag{16}$$

Therefore, the free gas reserves in the fractures and the matrix (G_{freep}) at the formation pressure (p) can be calculated as follows:

https://doi.org/10.1021/acsomega.2c01662
ACS Omega 2022, 7, 20927−20944

$$G_{freep} = \frac{\left[\begin{array}{l} G_m B_{gi} + \frac{G_m B_{gi}(1 - s_{fwc})\phi_f}{\phi_m} + \frac{G_m B_{gi}\rho_b\rho_{sc}}{\phi_m\rho_s} \\ (V_E(p_i) - V_E(p)) \\ -\frac{G_m B_{gi}\phi_{mt}}{\phi_m}(c_m + c_w s_{mwc})(p_i - p) \\ -\frac{G_m B_{gi}\phi_f}{\phi_m}(c_f + c_w s_{fwc})(p_i - p) \end{array}\right]}{B_g} \quad (17)$$

The adsorbed gas reserves (G_{ap}) at the formation pressure (p) are:

$$G_{ap} = \frac{G_m B_{gi}\rho_b}{\phi_m} V_E(p) \quad (18)$$

The dissolved gas reserves in kerogen (G_{dp}) at the formation pressure (p) are:

$$G_{dp} = c(p)\frac{G_m B_{gi} V_{diff}}{\phi_m} \quad (19)$$

According to the law of conservation of mass, the sum of the free gas reserves, adsorbed gas reserves, and dissolved gas reserves at the initial formation pressure is equal to the sum of the remaining adsorbed gas reserves, free gas reserves, dissolved gas reserves, and cumulative gas production at the current formation pressure. This can be expressed as follows:

$$G_{free} + G_a + G_d = G_{freep} + G_{ap} + G_{dp} + G_p \quad (20)$$

Substituting eqs 6, 7, 8, 17, 18, and 19 into eq 20, the material balance equation (as shown in Appendix B) is:

$$\frac{p}{Z^*} = \frac{p_i}{Z_i^*}\left(1 - \frac{G_p}{G}\right) \quad (21)$$

$$Z^* = \frac{Z}{\left[\begin{array}{l} 1 + \frac{(1 - s_{fwc})\phi_f}{\phi_m} - \frac{(c_m + c_w s_{mwc})\phi_{mt}}{\phi_m}(p_i - p) \\ -\frac{(c_f + c_w s_{fwc})\phi_f}{\phi_m}(p_i - p) \\ +\frac{\rho_b\rho_{sc}}{\phi_m\rho_s}(V_E(p_i) - V_E(p)) + \frac{\rho_b p_{sc} ZT}{\phi_m p Z_{sc} T_{sc}} V_E(p) \\ +\frac{p_{sc} ZT}{\phi_m p Z_{sc} T_{sc}} c(p) V_{diff} \end{array}\right]} \quad (22)$$

$$G = G_m\frac{Z_i}{Z_i^*} \quad (23)$$

Considering the free gas in the matrix and fractures, the change volume of the adsorbed phase, the adsorbed gas, and the dissolved gas in the kerogen, the comprehensive compressibility c_t^* can be calculated using eq 24, as shown in Appendix B.

$$c_t^* = c_g(s_{free} + C_{mf} + C_{ad} + C_a + C_d) + \frac{dC_{mf}}{dp} + \frac{dC_{ad}}{dp} + \frac{dC_a}{dp} + \frac{dC_d}{dp} \quad (24)$$

$$s_{free} = 1 + \frac{(1 - s_{fwc})\phi_f}{\phi_m} \quad (25)$$

$$C_{mf} = -\frac{(c_m + c_w s_{mwc})\phi_{mt}}{\phi_m}(p_i - p) - \frac{(c_f + c_w s_{fwc})\phi_f}{\phi_m}(p_i - p) \quad (26)$$

$$C_{ad} = \frac{\rho_b\rho_{sc}}{\phi_m\rho_s}(V_E(p_i) - V_E(p)) \quad (27)$$

$$C_a = \frac{\rho_b p_{sc} ZT}{\phi_m p Z_{sc} T_{sc}} V_E(p) \quad (28)$$

$$C_d = \frac{p_{sc} ZTV_{diff}}{\phi_m p Z_{sc} T_{sc}} c(p) \quad (29)$$

$$\frac{dC_{ad}}{dp} = -\frac{\rho_b\rho_{sc}}{\phi_m\rho_s}\frac{V_L p_L}{(p + p_L)^2} \quad (30)$$

$$\frac{dC_a}{dp} = \frac{\rho_b p_{sc}}{\phi_m Z_{sc} T_{sc}}\frac{T}{pZ}\left(\frac{dV_E(p)}{dp} - c_g V_E(p)\right) \quad (31)$$

$$\frac{dC_d}{dp} = \frac{p_{sc} V_{diff}}{\phi_m Z_{sc} T_{sc}}\frac{T}{pZ}\left(\frac{dc(p)}{dp} - c_g c(p)\right) \quad (32)$$

Considering eqs 12 and 14, the following formula can be obtained:

$$\frac{dC_{mf}}{dp} = \frac{\phi_{mt}}{\phi_m}[c_m(1 - c_m(p_i - p)) + c_w s_{mwc}(1 + c_w(p_i - p))] + \frac{\phi_f}{\phi_m}[c_f(1 - c_f(p_i - p)) + c_w s_{fwc}(1 + c_w(p_i - p))] \quad (33)$$

Considering the fluctuating flow and pressure during the production process, the material balance pseudotime[16] t_{ca}^* can be expressed as:

$$t_{ca}^* = \frac{c_{ti}^*\mu_i}{q(t)}\int_0^t \frac{q(t)}{\bar{\mu}\bar{c}_t^*}dt \quad (34)$$

The pseudopressure $m(p)$ can be expressed as:

$$m(p) = 2\int_{0.101}^{p}\frac{p}{\mu Z}dp \quad (35)$$

After derivations (as shown in Appendix B), the following expression can be obtained:

$$\frac{m(p_i) - m(p_{wf})}{q(t)} = \frac{2p_i}{c_{ti}^*\mu_i Z_i^* G} t_{ca}^* + b_{pss} \quad (36)$$

https://doi.org/10.1021/acsomega.2c01662
ACS Omega 2022, 7, 20927−20944

$$b_{pss} = \frac{p_{sc}T}{\alpha\pi T_{sc}k_{av}h}\left[\ln\left(\frac{r_e}{r_w}\right) - \frac{3}{4}\right] \quad (37)$$

Furthermore, the flowing material balance equation (as shown in Appendix B) can be obtained as follows:

$$\frac{q}{m(p_i) - m(p_{wf})} = \frac{1}{b_{pss}} - \frac{1}{b_{pss}G}\frac{m(p_i) - m(p)}{m(p_i) - m(p_{wf})}G \quad (38)$$

A straight line of $\frac{q}{m(p_i) - m(p_{wf})}$ versus $\frac{m(p_i) - m(p)}{m(p_i) - m(p_{wf})}G$ as shown in Figure 4, the slope k, and intercept b can be obtained:

$$k = -\frac{1}{b_{pss}G} \quad (39)$$

$$b = \frac{1}{b_{pss}} \quad (40)$$

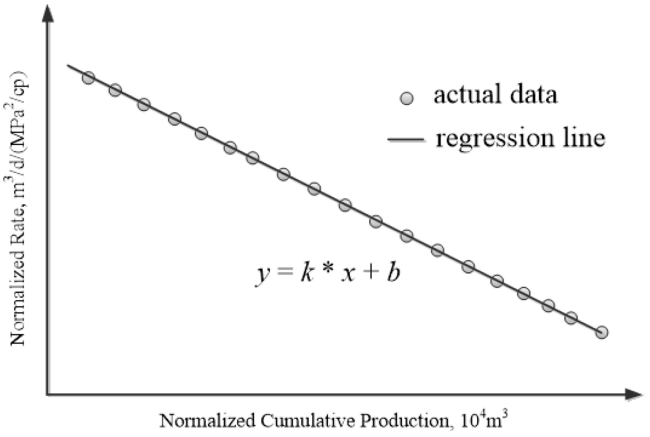

Figure 4. Schematic diagram of OGIP calculation using the flowing material balance method.

OGIP can be calculated as follows:

$$G = -\frac{b}{k} \quad (41)$$

To solve the difficulty in obtaining the accurate average formation pressure during the calculation of OGIP, the OGIP is first guessed and then iteratively solved by comparison with the calculation results from the proposed material balance equations. The flowchart is shown in Figure 5, and the specific steps are as follows:

(1) Assume the reserves G for single well.
(2) The average formation pressure p can be calculated using eq 21.
(3) Pseudopressure $m(p)$ can be calculated using eq 35.
(4) Calculate the normalized cumulative production $\frac{m(p_i) - m(p)}{m(p_i) - m(p_{wf})}G$.
(5) Calculate the normalized rate $\frac{q}{m(p_i) - m(p_{wf})}$.
(6) Draw a straight line of $\frac{q}{m(p_i) - m(p_{wf})}$ versus $\frac{m(p_i) - m(p)}{m(p_i) - m(p_{wf})}G$, and the slope k and intercept b are obtained to calculate G_{new} using eq 41.
(7) The calculated value G_{new} is compared with the hypothetical value G; if the accuracy requirement is satisfied, accept the calculated value G_{new}, otherwise go to (1), replace the hypothetical value G with the calculated value G_{new}, and recalculate it until the accuracy requirement is satisfied.

Fetkovich's curves can also be used to calculate OGIP.[34] By dividing both sides of eq 36 by b_{pss} and calculating the reciprocal, it can be obtained:

$$\frac{q(t)b_{pss}}{m(p_i) - m(p_{wf})} = \frac{1}{\frac{2p_i}{b_{pss}c_{ti}^*\mu_i Z_i^* G}t_{ca}^* + 1} \quad (42)$$

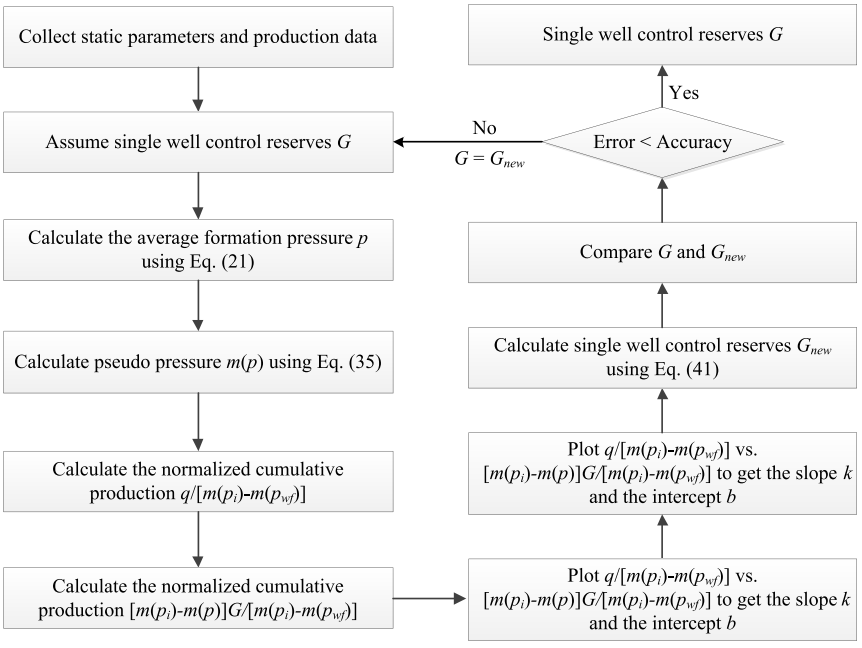

Figure 5. Solution procedure of the flowing material balance calculation for the OGIP of a single well.

https://doi.org/10.1021/acsomega.2c01662
ACS Omega 2022, 7, 20927−20944

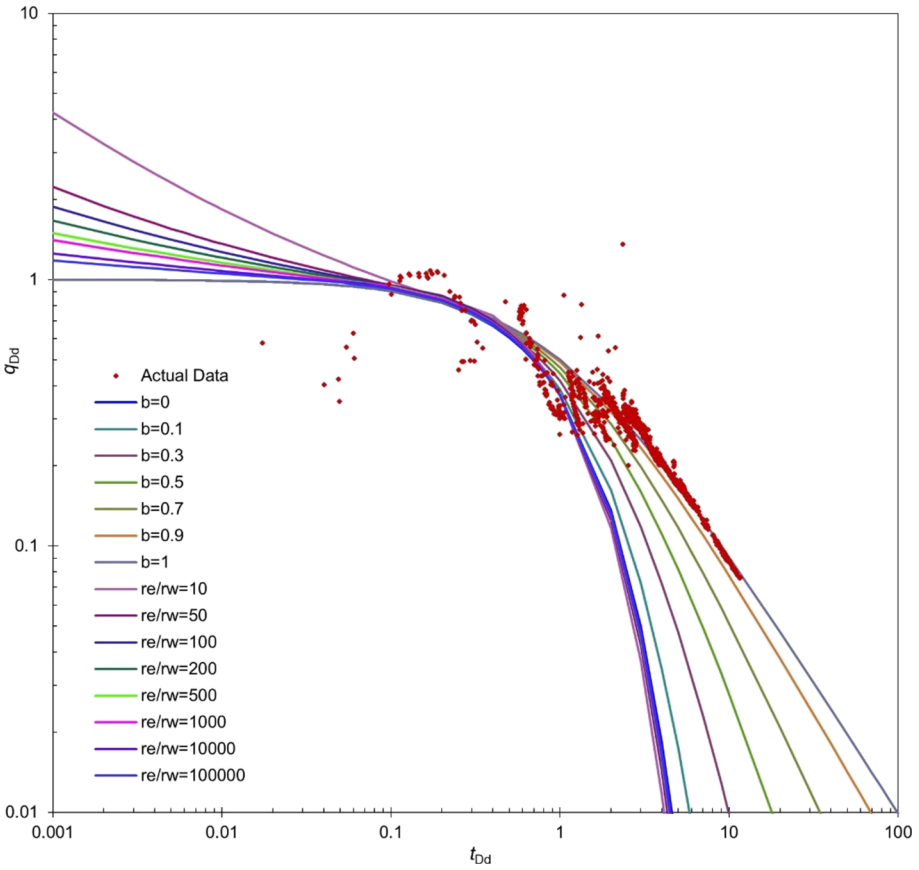

Figure 6. Matching plot of $q_g(t)/[m(p_i) - m(p_{wf})]$ versus t_{ca}^* on harmonic decline ($b = 1$) stems of Fetkovich's type curves to establish match points. Reprinted (adapted or reprinted in part) with permission from ref 34.

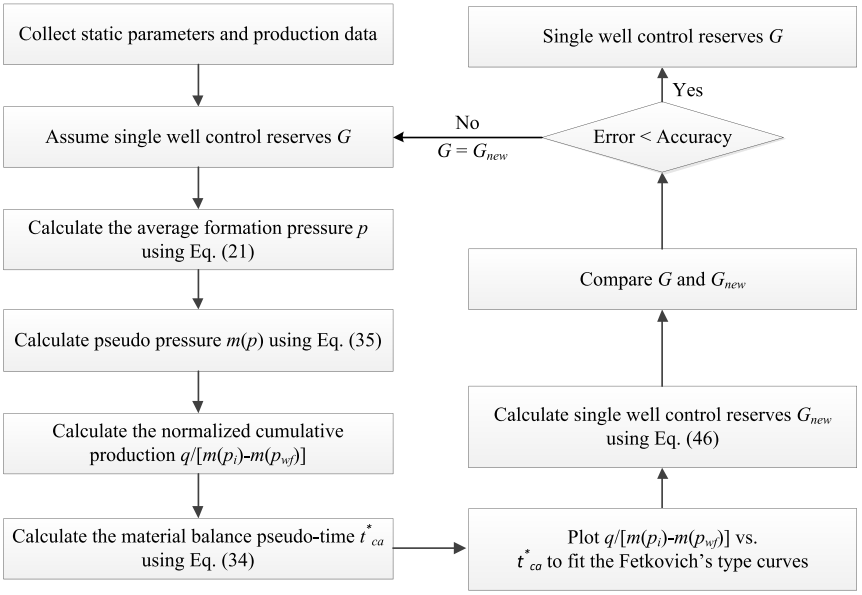

Figure 7. Solution procedure of fitting Fetkovich's type curves to calculate the OGIP of a single well.

Equation 42 can also be sorted into the form of a harmonic decline curve as follows:

$$q_{Dd} = \frac{1}{1 + t_{Dd}} \tag{43}$$

where,

$$q_{Dd} = \frac{q(t) b_{pss}}{m(p_i) - m(p_{wf})} \tag{44}$$

$$t_{Dd} = \frac{2p_i}{b_{pss} c_{ti}^* \mu_i Z_i^* G} t_{ca}^* \tag{45}$$

https://doi.org/10.1021/acsomega.2c01662
ACS Omega 2022, 7, 20927−20944

Using the line of $\frac{q(t)}{m(p_i)-m(p_{wf})}$ versus t_{ca}^* as shown in Figure 6 and fitting Fetkovich's type curves, the OGIP can be calculated as follows:

$$G = \frac{\left\{\frac{q(t)}{[m(p_i)-m(p_{wf})]}\right\}_{match}}{(q_{Dd})_{match}} \frac{2p_i}{Z_i^* \mu_i c_{ti}^*} \frac{(t_{ca}^*)_{match}}{(t_{Dd})_{match}} \quad (46)$$

The reserve can be calculated by fitting Fetkovich's type curves according to the following steps as shown in Figure 7.

(1) Assume the reserves G for single well.
(2) The average formation pressure p can be calculated using eq 21.
(3) Pseudopressure $m(p)$ can be calculated using eq 35.
(4) Calculate the normalized rate $\frac{q}{m(p_i)-m(p_{wf})}$.
(5) Calculate the material balance pseudotime t_{ca}^* according to eq 34.
(6) Draw a line of $\frac{q(t)}{m(p_i)-m(p_{wf})}$ versus t_{ca}^* and fit Fetkovich's type curves to calculate the G using eq 46.
(7) The calculated value G_{new} is compared with the hypothetical value G, if the accuracy requirement is satisfied, accept the calculated value G_{new}, otherwise go to (1), replace the hypothetical value G with the calculated value G_{new}, and recalculate it until the accuracy requirement is satisfied.

When the fractures are ignored, the equation proposed in this study can assume that:

$$\phi_f = 0 \quad (47)$$

$$c_f = 0 \quad (48)$$

When the dissolved gas in kerogen is not considered, the equations proposed in this study can assume that:

$$c(p) = 0 \quad (49)$$

When the volume of the adsorbed phase is not considered, the equation proposed in this study can assume that:

$$\rho_{sc} = 0 \quad (50)$$

3. RESULTS AND DISCUSSION

3.1. Validation of the Proposed Method for Shale Gas Reservoirs. To study the application of the method proposed in this study, the Fuling Shale Gas Field in southwest China is selected for research. The ratio between pore pressure to hydrostatic pressure is 1.41∼1.45, and the reservoir temperature is 85.99 °C. The thickness of the main layer is 38 m.

This study uses the JY1HF well for calculation, which has a long production time and has reached the pseudo-steady state flow stage. The rock and fluid properties are listed in Table 1 and the adsorption data and the properties of shale gas are shown in Figures 8 and 9, respectively.

Using properties of shale gas, rock and fluid parameters, and production dynamic data, the reserves can be calculated according to the steps proposed in Figure 5. The calculation results of the method proposed in this study and Clarkson's method are compared with the real reservoir to verify the accuracy of the proposed method, as shown in Figures 10 and 11 and Table 2.

Table 1. Rock and Fluid Properties of a Shale Gas Reservoir of JY1HF

parameters	values
s_{fwc}	0.0
s_{mwc}	0.3
V_L, m^3/t	1.4524
p_L, MPa	19.95
ϕ_{mt}	0.044
ϕ_f	0.001
ϕ_{org}	0.005
TOC, %	3.88
ρ_b, g/cm^3	2.650
ρ_{ko}, g/cm^3	1.325
T, K	354.07
p_i, MPa	40.00
ρ_{sc}, g/cm^3	0.00077
ρ_s, g/cm^3	0.340
c_m, MPa^{-1}	0.000435
c_w, MPa^{-1}	0.000435
c_f, MPa^{-1}	0.004350
A, km^2	0.06
h, m	38

From Table 2, it can be observed that the method proposed in this study has a smaller deviation compared with the actual value. The control volume calculated by the method proposed in this study is 2302.90 × 10^4 m^3 and the actual control volume is 2280.00 × 10^4 m^3, and the relative deviation is only 1.00%, while the control volume calculated by Clarkson's method is 2744.99 × 10^4 m^3 and the relative deviation is 20.39%, suggesting the accuracy of the proposed model. For the method proposed in this study, the calculated OGIP is 34633.90 × 10^4 m^3 including (a) the calculated free gas reserves in the fracture of 831.02 × 10^4 m^3 and a proportion of 2.40%; (b) calculated initial free gas reserves in the matrix of 18770.57 × 10^4 m^3, accounting for 54.20%; (c) calculated initial adsorbed gas reserves of 6054.14 × 10^4 m^3, accounting for 17.48%; and (d) calculated initial dissolved gas reserves of 8978.18 × 10^4 m^3, accounting for 25.92%.

With consideration of the free gas in the fractures, the dissolved gas in the kerogen, and the volume of the adsorbed phase, the calculated control area is closer to the actual situation, indicating that it is necessary and reasonable to consider these factors in the proposed method. Moreover, the dissolved gas in kerogen accounts for 25.92%, which is relatively large and cannot be ignored.

3.2. Forecast Future Gas Rate. The related expression between BHP and gas production can be determined utilizing the material balance method (eq 21) and the flowing material balance method (eq 38) described in this study. The steps (Figure 12) for forecasting the daily gas production rate are as follows:

(1) Calculate b_{pss} and G in eq 38 using historical production data.
(2) Assume the next moment's gas production q_g^{n+1}.
(3) Calculate the next moment's cumulative gas production G_p^{n+1}.

$$G_p^{n+1} = G_p^n + q_g^{n+1} \quad (51)$$

(4) Calculate the average formation pressure using eq 21.

https://doi.org/10.1021/acsomega.2c01662
ACS Omega 2022, 7, 20927−20944

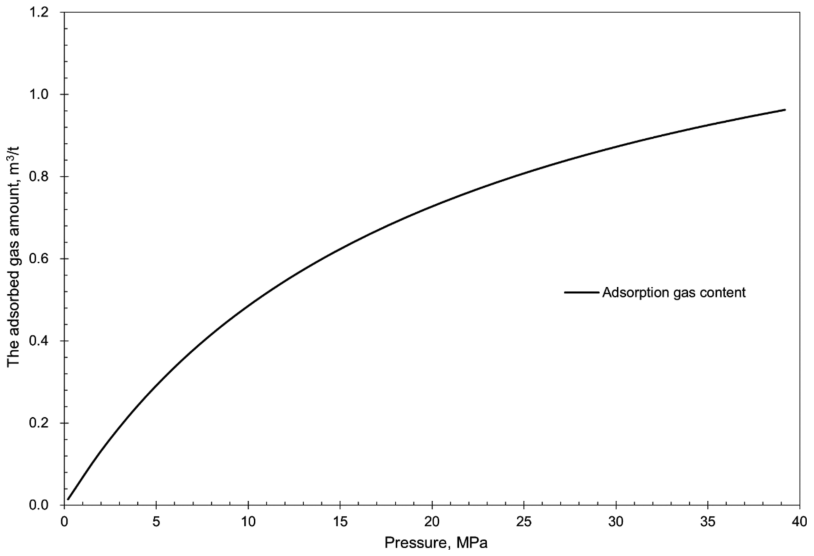

Figure 8. Adsorbed gas amount of pure CH_4 for JY1HF.

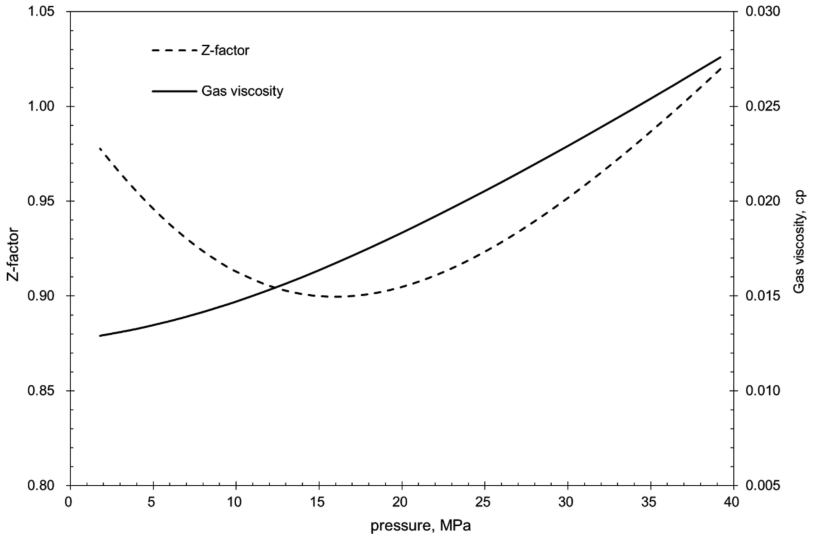

Figure 9. Properties of the JY1HF shale gas well.

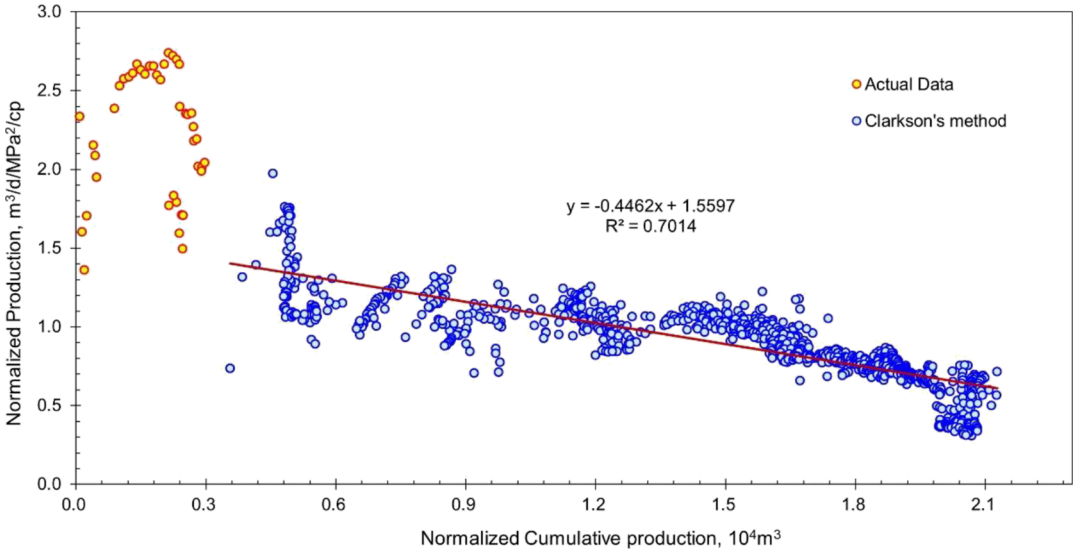

Figure 10. Flowing material balance calculation results of Clarkson's method.

https://doi.org/10.1021/acsomega.2c01662
ACS Omega 2022, 7, 20927−20944

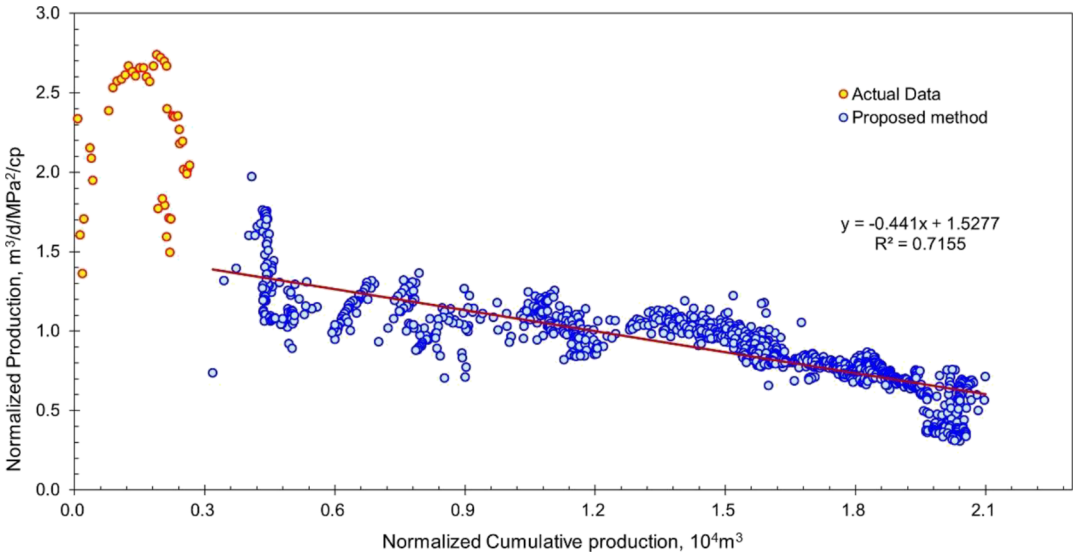

Figure 11. Flowing material balance calculation results of the proposed method.

Table 2. Comparison Result of the Proposed Method and Clarkson's Method

		proposed method		Clarkson's method	
parameters	actual value	evaluated value	relative deviation (%)	evaluated value	relative deviation (%)
Ah, 10^4 m^3	2280.00	2302.90	−1.00	2744.99	20.39
A, km^2	0.6000	0.6060	−1.00	0.7224	20.40
G_m, 10^4 m^3	18583.93	18770.57	−1.00	27735.27	49.24
G_f, 10^4 m^3	822.75	831.02	−1.01		
G_a, 10^4 m^3	5993.94	6054.14	−1.00	7216.35	20.39
G_d, 10^4 m^3	8888.91	8978.18	−1.00		
G, 10^4 m^3	34289.52	34633.9	−1.00	34951.61	1.93

(5) Apply eq 38 to calculate gas production q_{gnew}^{n+1} based on a given BHP (p_{wf}^{n+1}).
(6) If $abs(q_g^{n+1} - q_{gnew}^{n+1}) < eps$, stop the iteration. Otherwise, make $q_g^{n+1} = q_{gnew}^{n+1}$, return to step (3), and retry the calculation.

Through these steps, the future production performance can be predicted using BHP. The fitting and prediction results of gas production are shown in Figure 13. The accurate matched results suggest that the model can be used to predict future gas production. Assuming that the economic limit of the gas production rate is 5000 m^3/d, the final cumulative gas production will be 23098.25 × 10^4 m^3, and the gas recovery of JY1HF will be 66.70%.

3.3. Sensitivity Analyses. Sensitivity analyses were carried out in this study to determine the sensitivity parameters that affect the calculation results of reserves. Langmuir volume, Langmuir pressure, total organic carbon (TOC), and fracture porosity were analyzed, respectively.

Assuming that the Langmuir volume changes from 0.4 to 2.8 m^3/t, different reserves were calculated as shown in Figure 14. It was observed that the free gas reserves in the matrix reduced by 18.69%, the reserves of adsorbed gas increased by 759%, the free gas reserves in the fractures increased by 22.80%, and the reserves of dissolved gas increased by 5.70%. The Langmuir volume mainly affects the adsorbed gas reserves. The larger the Langmuir volume, the higher the adsorbed gas reserves.

Assuming that the Langmuir pressure changes from 10.00 to 30.00 MPa, different reserves were calculated as shown in Figure 15. It was observed that the free gas reserves in the matrix increased by 0.34%, the reserves of adsorbed gas decreased by 32.65%, the free gas reserves in the fractures decreased by 7.28%, and the reserves of dissolved gas decreased by 4.48%. The Langmuir pressure mainly affects the adsorbed gas reserves, but the impact was not great.

Assuming that the TOC changes from 2.00 to 6.00%, different reserves were calculated as shown in Figure 16. It was observed

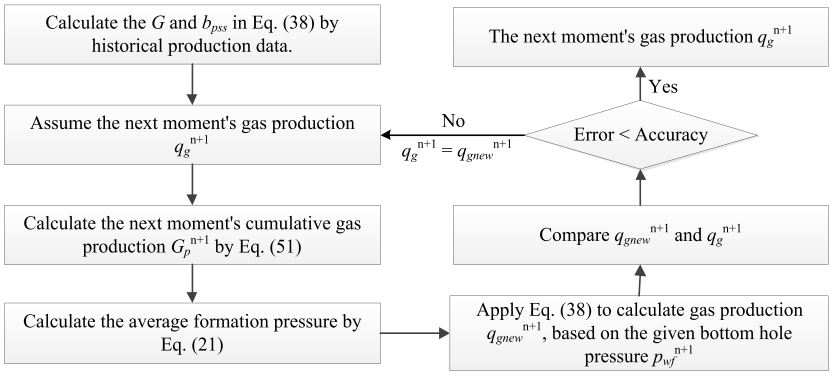

Figure 12. Solution procedure of the flowing material balance calculation for the gas production rate of a single well.

https://doi.org/10.1021/acsomega.2c01662
ACS Omega 2022, 7, 20927−20944

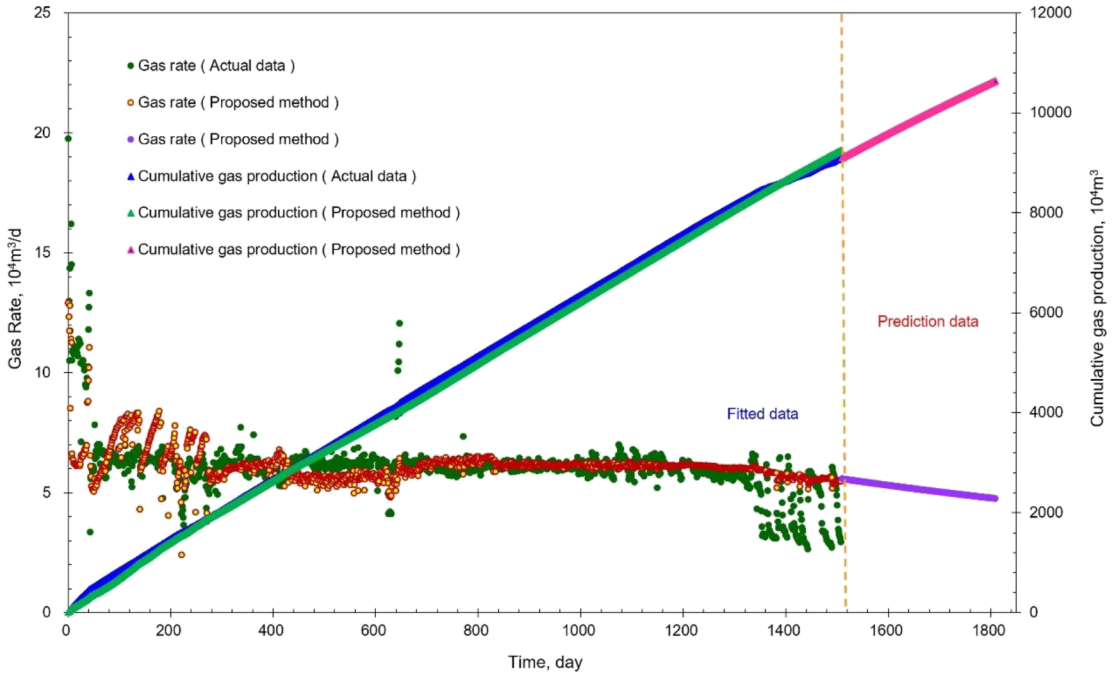

Figure 13. Fitting and prediction of production data for the JY1HF well.

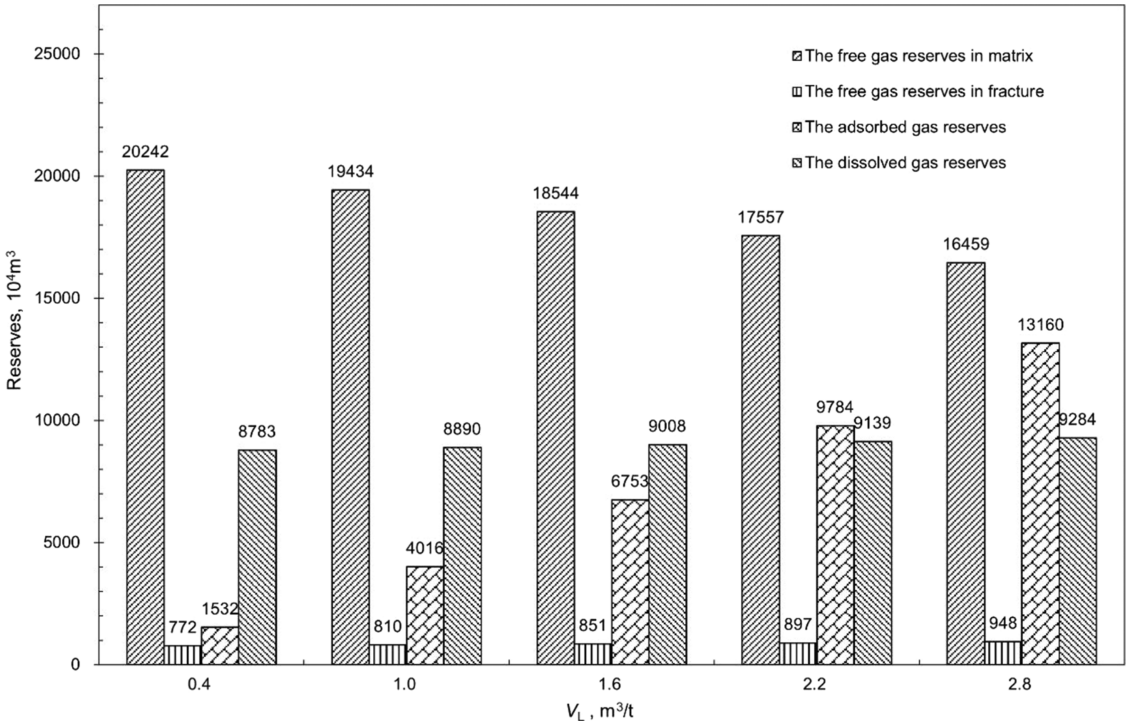

Figure 14. Calculation results of reserves for different Langmuir volumes.

that the free gas reserves in the matrix decreased by 33.57%, the reserves of adsorbed gas decreased by 33.57%, the free gas reserves in the fractures decreased by 33.49%, and the reserves of dissolved gas increased by 149.39%. The TOC mainly affects the dissolved gas reserves, and as the TOC increases, the reserves of dissolved gas will increase.

Assuming that the fracture porosity changes from 0.001 to 0.01, different reserves were calculated as shown in Figure 17. It was observed that the free gas reserves in the matrix decreased by 20.09%, the reserves of adsorbed gas decreased by 20.09%, the free gas reserves in the fractures increased by 698.66%, and the reserves of dissolved gas decreased by 20.09%. The fracture porosity mainly affects the free gas reserves in the fractures, and as the fracture porosity increases, the free gas reserves in the fracture will increase.

This study also demonstrates the influence of Langmuir pressure, Langmuir volume, and adsorbed phase density on the porosity of the adsorbed phase. Assuming different Langmuir pressures, the porosity of the free gas in the matrix can be calculated, and the results are shown in Table 3. It was observed

https://doi.org/10.1021/acsomega.2c01662
ACS Omega 2022, 7, 20927−20944

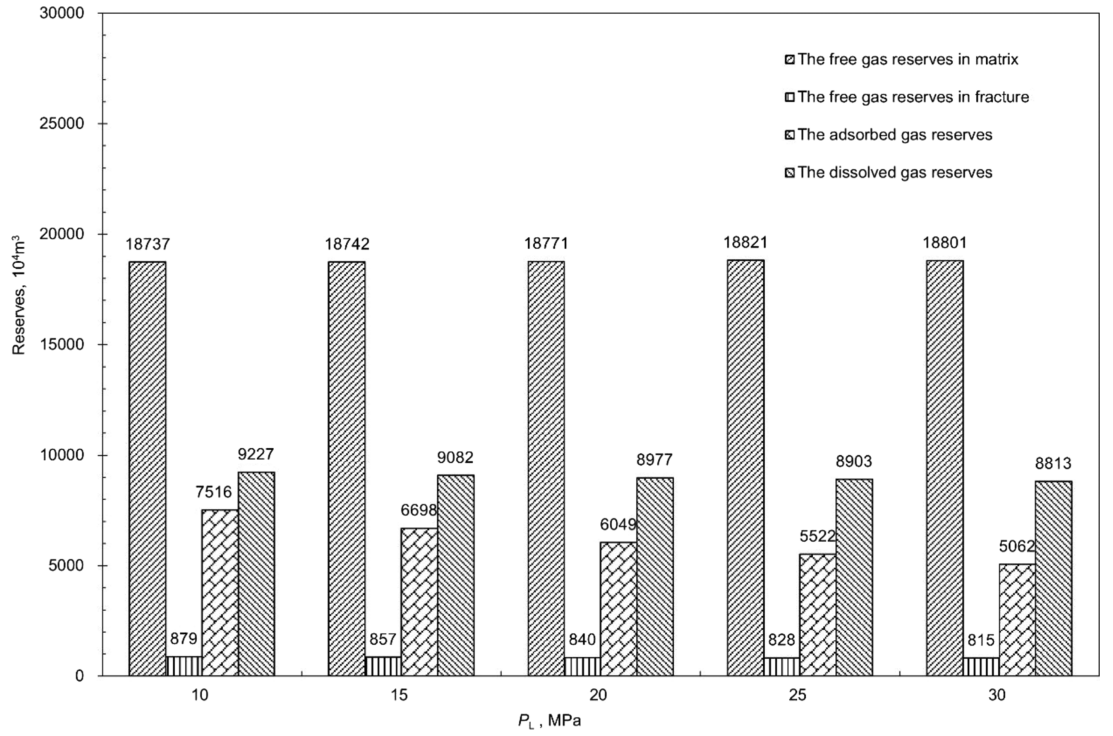

Figure 15. Calculation results of reserves for different Langmuir pressures.

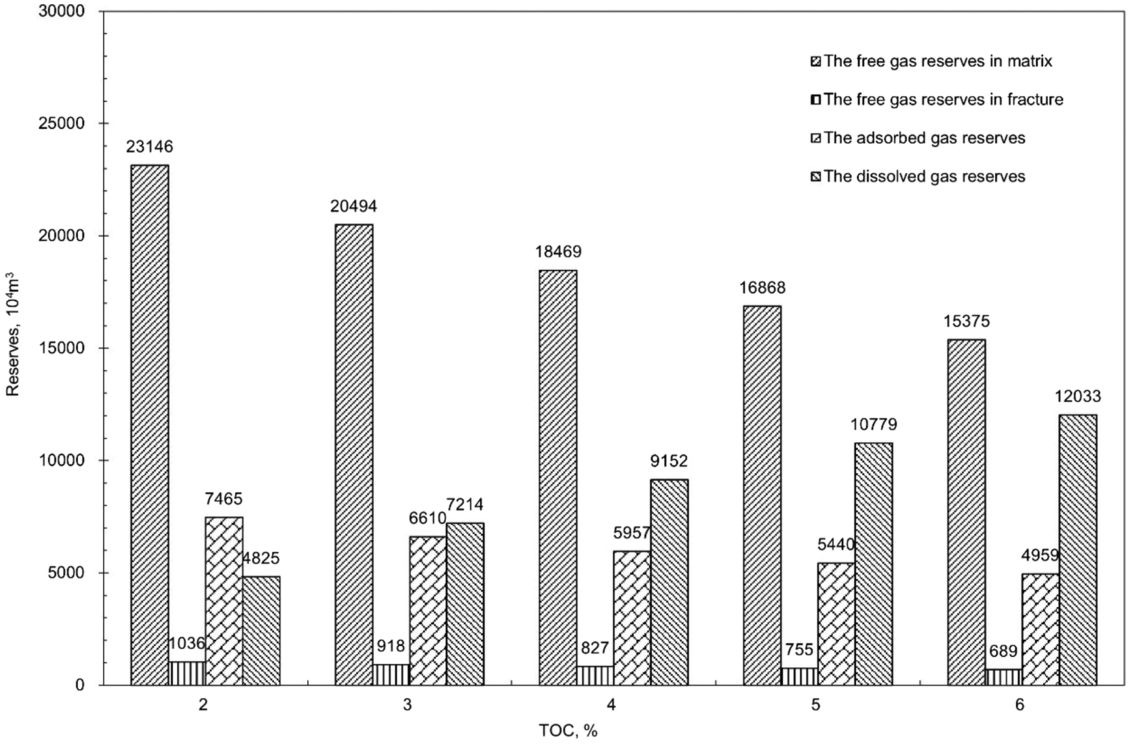

Figure 16. Calculation results of reserves for different TOCs.

that with the increase of Langmuir pressure, the difference in the free gas porosity in the matrix became smaller. Therefore, when the Langmuir pressure is large enough, the volume of the adsorbed phase can be ignored.

Assuming different Langmuir volumes, the porosity of the free gas in the matrix was calculated, and the results are shown in Table 4. It was observed that with the increase of Langmuir volume, the difference in the free gas porosity in the matrix became larger. Therefore, when the Langmuir volume is small enough, the volume of the adsorbed phase can be ignored.

Assuming different adsorbed phase densities, the porosity of the free gas in the matrix was calculated, and the results are shown in Table 5. It was observed that with the increase of adsorbed phase density, the difference in the free gas porosity in

https://doi.org/10.1021/acsomega.2c01662
ACS Omega 2022, 7, 20927−20944

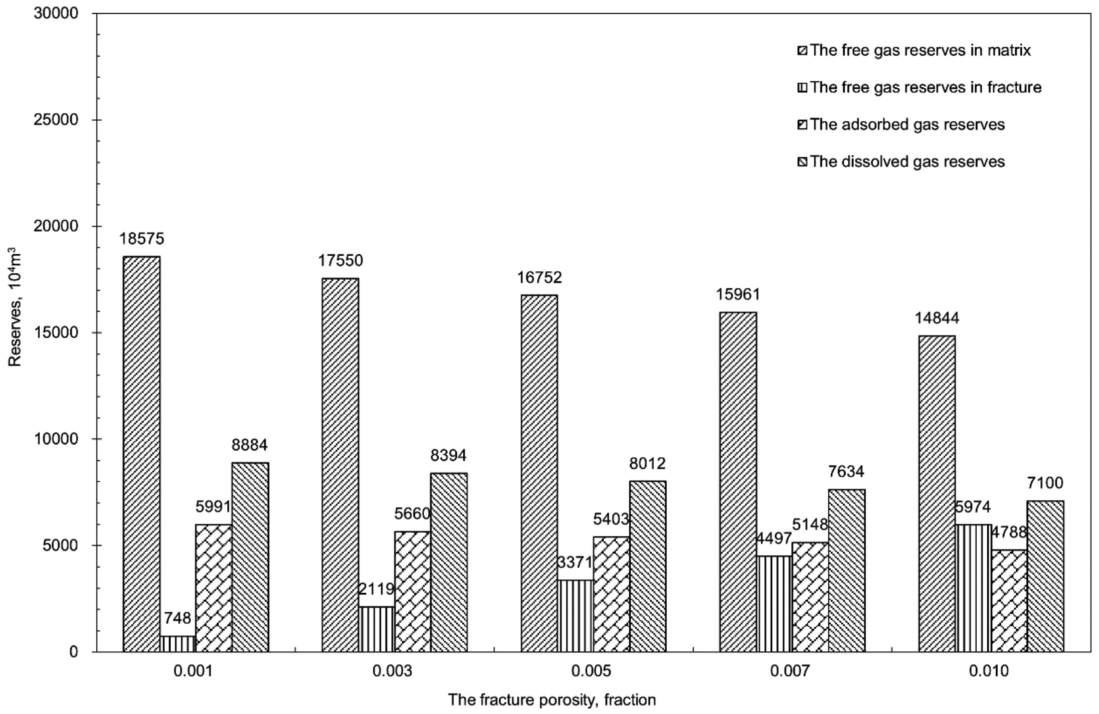

Figure 17. Calculation results of reserves for different fracture porosities.

Table 3. Free Gas Porosity in the Matrix for Different Langmuir Pressures

	free gas porosity in the matrix		
P_L (MPa)	considering the volume of the adsorbed phase	without considering the volume of the adsorbed phase	relative deviation (%)
10	0.0238	0.0308	−22.64
15	0.0245	0.0308	−20.58
20	0.0250	0.0308	−18.87
25	0.0254	0.0308	−17.42
30	0.0258	0.0308	−16.17
35	0.0262	0.0308	−15.09

Table 4. Free Gas Porosity in the Matrix for Different Langmuir Volumes

	free gas porosity in the matrix		
V_L (m^3/t)	considering the volume of the adsorbed phase	without considering the volume of the adsorbed phase	relative deviation (%)
0.50	0.0288	0.0308	−6.50
1.00	0.0268	0.0308	−13.00
1.50	0.0248	0.0308	−19.50
2.00	0.0228	0.0308	−26.00
2.50	0.0208	0.0308	−32.50
3.00	0.0188	0.0308	−39.00

Table 5. Free Gas Porosity in the Matrix for Different Adsorbed Phase Densities

	free gas porosity in the matrix		
ρ_s (g/m^3)	considering the volume of the adsorbed phase	without considering the volume of the adsorbed phase	relative deviation (%)
0.1	0.0110	0.0308	−64.20
0.2	0.0209	0.0308	−32.10
0.3	0.0242	0.0308	−21.40
0.4	0.0259	0.0308	−16.05
0.5	0.0268	0.0308	−12.84
0.6	0.0275	0.0308	−10.70

the matrix became smaller. Therefore, when the adsorbed phase density is large enough, the volume of the adsorbed phase can be ignored.

3.4. Discussion. To establish the material balance equation for OGIP calculation, the method proposed in this study integrates various factors (adsorbed gas in the matrix, dissolved gas in kerogen, free gas in the matrix, free gas in fractures, adsorbed phase occupying pore volume, and irreducible water expansion). The advantage of this model over earlier models is that the factors addressed are more extensive, and the calculation outputs are more accurate following example verification. The adsorption model and multiscale gas fluid flow are considered to describe the volume change of gas adsorption/desorption and gas dissolution. By rebuilding the pore volume model, the volume changes of gas in kerogen, matrix and fractures, the volume changes due to stress sensitivity and irreducible water expansion, and volume change due to adsorbed density change are considered. Fewer parameters (i.e., BHP, the gas production rate, and initial formation pressure) are required in this model, which compensate the time-consuming build-up well tests. However, there are numerous disadvantages in this study; important parameters such as fracture porosity, organic porosity, and adsorption phase density are difficult to obtain. The precision of these parameters is directly related to the accuracy of reserve evaluation. Furthermore, there are some limitations in this study, the solubility of dissolved gas in kerogen is referred to the empirical model of the solubility of methane in asphaltene proposed by Mehrotra and Svrcek,[33] and whether the coefficients in it are applicable to methane in kerogen needs to be investigated further. To achieve more accurate storage evaluation results, future studies should focus on the acquisition of fracture porosity, organic matter porosity, and adsorption

https://doi.org/10.1021/acsomega.2c01662
ACS Omega 2022, 7, 20927−20944

phase density as well as the calculation of methane solubility in kerogen.

4. SUMMARY AND CONCLUSIONS

This study follows the law of conservation of mass and establishes a material balance equation considering the free gas in the fracture and matrix, adsorbed gas in the matrix, dissolved gas, stress sensitivity, and irreducible water expansion. On this basis, considering double porosity and single permeability, a flowing material balance equation can be established under the pseudo-steady state. Through the calculation of examples, the following conclusions can be obtained.

(1) The application results in actual gas reservoirs show that the calculation results of the flowing material balance method proposed in this study are more accurate compared with Clarkson's method.
(2) Dissolved gas accounts for 25.92%, indicating that dissolved gas is an important way of gas storage mechanism and cannot be ignored.
(3) The method proposed in this study can predict gas production when the BHP is known, which can be used as a reference for the design of development plans.
(4) The greater the fracture porosity, the greater the free gas reserves in the fracture. The free gas in fractures cannot be ignored when calculating reserves for fractured shale gas reservoirs.
(5) The larger the Langmuir volume, the higher the adsorbed gas reserves. The greater the TOC, the greater the dissolved gas reserves.
(6) The volume of adsorbed phase decreases as the Langmuir pressure and adsorbed phase density increase, and it increases as the Langmuir volume increases. The pore volume occupied by the adsorbed phase could be neglected if the Langmuir pressure and density of the adsorbed phase are ultimately large or the Langmuir volume is ultimately small.

APPENDIX A

The fracture porosity is defined as:

$$\phi_f = \frac{V_f}{V_b} \tag{A1}$$

The matrix porosity is expressed as follows:

$$\phi_{mt} = \frac{V_p}{V_b} \tag{A2}$$

Then, the volume of the fracture can be calculated as:

$$V_f = \frac{V_p \phi_f}{\phi_{mt}} \tag{A3}$$

The matrix pore volume is composed of three parts: the pore volume occupied by the free gas, adsorbed phase, and irreducible water, which is expressed as follows:

$$V_p = V_g + V_a + V_{wi} \tag{A4}$$

The pore volume occupied by irreducible water is expressed as follows:

$$V_{wi} = V_p s_{mwc} \tag{A5}$$

The pore volume occupied by the adsorbed phase is expressed as follows:

$$V_a = \frac{V_b \rho_b V_E(p_i) \rho_{sc}}{\rho_s} \tag{A6}$$

The pore volume occupied by free gas is expressed as follows:

$$V_g = G_m B_{gi} \tag{A7}$$

Substituting eqs A4, A5, A6, A7 into eq A3, the following relationship can be obtained:

$$\frac{G_m B_{gi}}{V_b} = \phi_{mt}(1 - s_{mwc}) - \frac{\rho_b V_E(p_i) \rho_{sc}}{\rho_s} \tag{A8}$$

The porosity of free gas in the matrix can be defined as:

$$\phi_m = \phi_{mt}(1 - s_{mwc}) - \frac{\rho_b V_E(p_i) \rho_{sc}}{\rho_s} \tag{A9}$$

The total volume of rock is expressed as follows:

$$V_b = \frac{G_m B_{gi}}{\phi_m} \tag{A10}$$

Substituting eq A10 into eq A3, the fracture volume is expressed as follows:

$$V_f = \frac{G_m B_{gi} \phi_f}{\phi_m} \tag{A11}$$

APPENDIX B

Define the following expression:

$$H = \frac{\rho_b \rho_{sc}}{\phi_m \rho_s} \tag{B1}$$

$$F = \frac{(1 - s_{fwc})\phi_f}{\phi_m} \tag{B2}$$

$$c_M = \frac{(c_m + c_w s_{mwc})\phi_{mt}}{\phi_m} \tag{B3}$$

$$c_F = \frac{c_f + c_w s_{fwc}}{1 - s_{fwc}} F \tag{B4}$$

Then, substituting eqs 6, 7, 8, 17, 18, 19, and B1, B2, B3, B4 into eq 21, we obtain

$$G_m + G_m F + \frac{G_m B_{gi} \rho_b}{\phi_m} V_E(p_i) + \frac{G_m B_{gi}}{\phi_m} c(p_i) V_{diff} = \frac{G_m B_{gi} \rho_b}{\phi_m} V_E(p) + \frac{G_m B_{gi}}{\phi_m} c(p) V_{diff} + G_p + \frac{\left[G_m B_{gi} + G_m B_{gi} F + G_m B_{gi} H(V_E(p_i) - V_E(p)) - G_m B_{gi} c_M(p_i - p) - G_m B_{gi} c_F(p_i - p) \right]}{B_g} \tag{B5}$$

Multiply both sides by B_g at the same time to get the following formula:

https://doi.org/10.1021/acsomega.2c01662
ACS Omega 2022, 7, 20927−20944

$$G_m B_g + G_m B_g F + \frac{G_m B_{gi} \rho_b B_g}{\phi_m} V_E(p_i) + \frac{G_m B_{gi} B_g}{\phi_m} c(p_i) V_{diff}$$
$$= G_m B_{gi} + G_m B_{gi} F + G_m B_{gi} H(V_E(p_i) - V_E(p))$$
$$- G_m B_{gi}(c_M + c_F)(p_i - p) + \frac{G_m B_{gi} \rho_b B_g}{\phi_m} V_E(p)$$
$$+ \frac{G_m B_{gi} B_g}{\phi_m} c(p) V_{diff} + G_p B_g \quad (B6)$$

Organize and get the following formula:

$$G_m B_{gi} + G_m B_{gi} H(V_E(p_i) - V_E(p)) + G_m B_{gi} F$$
$$- G_m B_{gi}(c_M + c_F)(p_i - p)$$
$$= G_m B_g + G_m B_g F + \frac{G_m B_{gi} \rho_b B_g}{\phi_m}(V_E(p_i) - V_E(p)) +$$
$$\frac{G_m B_{gi} B_g V_{diff}}{\phi_m}(c(p_i) - c(p)) - G_p B_g \quad (B7)$$

Divide both sides by $G_m B_{gi}$ at the same time to get the following formula:

$$1 + H(V_E(p_i) - V_E(p)) + F - (c_M + c_F)(p_i - p)$$
$$+ \frac{\rho_b B_g V_E(p)}{\phi_m} + \frac{B_g c(p) V_{diff}}{\phi_m}$$
$$= \frac{B_g}{B_{gi}} + \frac{B_g}{B_{gi}} F + \frac{\rho_b B_g V_E(p_i)}{\phi_m} + \frac{B_g c(p_i) V_{diff}}{\phi_m} - \frac{G_p B_g}{G_m B_{gi}} \quad (B8)$$

As known,

$$\frac{B_g}{B_{gi}} = \frac{Z}{p} \times \frac{p_i}{Z_i} \quad (B9)$$

Substituting eq B9 into eq B8, the following formula can be obtained:

$$1 + H(V_E(p_i) - V_E(p)) + F - (c_M + c_F)(p_i - p)$$
$$+ \frac{\rho_b B_g V_E(p)}{\phi_m} + \frac{B_g c(p) V_{diff}}{\phi_m}$$
$$= (1 + F)\frac{Z}{p}\frac{p_i}{Z_i} + \frac{\rho_b B_g V_E(p_i)}{\phi_m} + \frac{B_g c(p_i) V_{diff}}{\phi_m} - \frac{G_p}{G_m}\frac{Z}{p}\frac{p_i}{Z_i} \quad (B10)$$

Multiply both sides by $\frac{p}{Z}$ at the same time to get the following formula:

$$\frac{p}{Z}(1 + F) - \frac{p}{Z}(c_M + c_F)(p_i - p)$$
$$+ \frac{p}{Z} H(V_E(p_i) - V_E(p))$$
$$+ \frac{p}{Z}\frac{\rho_b B_g V_E(p)}{\phi_m} + \frac{p}{Z}\frac{B_g c(p) V_{diff}}{\phi_m}$$
$$= (1 + F)\frac{p_i}{Z_i} + \frac{p}{Z}\frac{\rho_b B_g V_E(p_i)}{\phi_m} + \frac{p}{Z}\frac{B_g c(p_i) V_{diff}}{\phi_m} - \frac{G_p}{G_m}\frac{p_i}{Z_i} \quad (B11)$$

Substituting eq B9 into eq B11, the following formula can be obtained:

$$\frac{p}{Z}\left[\begin{array}{l}(1 + F) - (c_M + c_F)(p_i - p) + \\ H(V_E(p_i) - V_E(p)) + \frac{\rho_b B_g V_E(p)}{\phi_m} \\ + \frac{B_g V_{diff} c(p)}{\phi_m}\end{array}\right]$$
$$= \frac{p_i}{Z_i}\left[(1 + F) + \frac{\rho_b B_{gi} V_E(p_i)}{\phi_m} + \frac{B_{gi} V_{diff} c(p_i)}{\phi_m}\right] - \frac{p_i}{Z_i}\frac{G_p}{G_m} \quad (B12)$$

Define the following expression:

$$Z^* = \frac{Z}{\left[\begin{array}{l}(1 + F) - (c_M + c_F)(p_i - p) + \\ H(V_E(p_i) - V_E(p)) + \frac{\rho_b B_g V_E(p)}{\phi_m} \\ + \frac{B_g c(p) V_{diff}}{\phi_m}\end{array}\right]} \quad (B13)$$

Substituting eq B13 into eq B12, the following formula can be obtained:

$$\frac{p}{Z^*} = \frac{p_i}{Z_i^*} - \frac{p_i}{Z_i}\frac{G_p}{G_m} \quad (B14)$$

As known,

$$G = G_m + G_f + G_a + G_d$$
$$= G_m\left(1 + F + \frac{\rho_b B_{gi} V_E(p_i)}{\phi_m} + \frac{B_{gi} c(p_i) V_{diff}}{\phi_m}\right) = G_m \frac{Z_i}{Z_i^*} \quad (B15)$$

Substituting eq B15 into eq B14, the following formula can be obtained:

$$\frac{p}{Z^*} = \frac{p_i}{Z_i^*} - \frac{p_i}{Z_i^*}\frac{G_p}{G} \quad (B16)$$

As known,

$$B_g = \frac{p_{sc} Z T}{p Z_{sc} T_{sc}} \quad (B17)$$

Substituting eq B17 into eq B13, the following formula can be obtained:

https://doi.org/10.1021/acsomega.2c01662
ACS Omega 2022, 7, 20927−20944

$$Z^*=\frac{Z}{\left[\begin{array}{l}1+\frac{(1-s_{fwc})\phi_f}{\phi_m}-\frac{(c_m+c_w s_{mwc})\phi_{mt}}{\phi_m}(p_i-p)\\ -\frac{(c_f+c_w s_{fwc})\phi_f}{\phi_m}(p_i-p)+\\ \frac{\rho_b p_{sc}}{\phi_m \rho_s}(V_E(p_i)-V_E(p))+\frac{\rho_b p_{sc} ZT}{\phi_m p Z_{sc} T_{sc}}V_E(p)\\ +\frac{p_{sc} ZT}{\phi_m p Z_{sc} T_{sc}}c(p)V_{diff}\end{array}\right]} \tag{B18}$$

Define the following expression:

$$s_{free}=1+\frac{(1-s_{fwc})\phi_f}{\phi_m} \tag{B19}$$

$$C_{mf}=-\frac{(c_m+c_w s_{mwc})\phi_{mt}}{\phi_m}(p_i-p)-\frac{(c_f+c_w s_{fwc})\phi_f}{\phi_m}(p_i-p) \tag{B20}$$

$$C_{ad}=\frac{\rho_b \rho_{sc}}{\phi_m \rho_s}(V_E(p_i)-V_E(p)) \tag{B21}$$

$$C_a=\frac{\rho_b p_{sc} ZT}{\phi_m p Z_{sc} T_{sc}}V_E(p) \tag{B22}$$

$$C_d=\frac{p_{sc} ZT}{\phi_m p Z_{sc} T_{sc}}c(p)V_{diff} \tag{B23}$$

Substituting eqs B19, B20, B21, B22, and B23 into eq B18, the following formula can be obtained:

$$Z^*=\frac{Z}{s_{free}+C} \tag{B24}$$

$$C=C_{mf}+C_{ad}+C_a+C_d \tag{B25}$$

The pseudopressure can be expressed as:

$$m(p)=2\int_{0.101}^{p}\frac{p}{\mu Z}dp \tag{B26}$$

Differentiating eq B16 with respect to time, the following formula can be obtained:

$$\frac{d\left(\frac{p}{Z^*}\right)}{dt}=\frac{d\left(\frac{p}{Z^*}\right)}{dp}\frac{dp}{dm}\frac{dm}{dt}=-\frac{p_i q_g}{Z_i^* G} \tag{B27}$$

Then,

$$\frac{dm}{dt}=\frac{-\frac{p_i q_g}{Z_i^* G}\frac{2p}{\mu Z}}{\frac{d\left(\frac{p}{Z^*}\right)}{dp}}=\frac{-\frac{2p_i q_g}{Z_i^* G\mu}}{(s_{free}+C)\left(\frac{1}{p}-\frac{1}{Z^*}\frac{dZ^*}{dp}\right)} \tag{B28}$$

$$\frac{dZ^*}{dp}=\frac{(s_{free}+C)\frac{dZ}{dp}-Z\frac{dC}{dp}}{(s_{free}+C)^2} \tag{B29}$$

Substituting eqs B24 and B29 into eq B28, the following formula can be obtained:

$$\frac{dm}{dt}=\frac{-\frac{2p_i q_g}{Z_i^* G\mu}}{c_t^*} \tag{B30}$$

$$c_t^*=c_g(s_{free}+C)+\frac{dC}{dp} \tag{B31}$$

$$\frac{dC}{dp}=\frac{dC_{mf}}{dp}+\frac{dC_{ad}}{dp}+\frac{dC_a}{dp}+\frac{dC_d}{dp} \tag{B32}$$

Equation B33 can be obtained from eqs 11 and 13 as follows:

$$\frac{dC_{mf}}{dp}=\frac{\phi_{mt}}{\phi_m}[c_m(1-c_m(p_i-p))+c_w s_{mwc}(1+c_w(p_i-p))]+\frac{\phi_f}{\phi_m}[c_f(1-c_f(p_i-p))+c_w s_{fwc}(1+c_w(p_i-p))] \tag{B33}$$

$$\frac{dC_{ad}}{dp}=-\frac{\rho_b \rho_{sc}}{\phi_m \rho_s}\frac{dV_E(p)}{dp} \tag{B34}$$

$$\frac{dC_a}{dp}=\frac{\rho_b p_{sc}}{\phi_m Z_{sc} T_{sc}}\frac{T}{pZ}\left(\frac{dV_E(p)}{dp}-c_g V_E(p)\right) \tag{B35}$$

$$\frac{dC_d}{dp}=\frac{p_{sc} V_{diff}}{\phi_m Z_{sc} T_{sc}}\frac{T}{pZ}\left(\frac{dc(p)}{dp}-c_g c(p)\right) \tag{B36}$$

Considering Langmuir isotherm adsorption, we obtain

$$\frac{dV_E(p)}{dp}=\frac{V_L p_L}{(p+p_L)^2} \tag{B37}$$

Differentiating the empirical formula for dissolved gases with respect to pressure, we obtain

$$\frac{dc(p)}{dp}=1.0732\left(b_2+\frac{b_3}{T}+\frac{2b_4}{T^2}p\right) \tag{B38}$$

In the pseudosteady state, for variable flow/variable pressure, the material balance pseudotime is introduced:

$$t_{ca}^*=\frac{c_{ti}^*\mu_i}{q(t)}\int_0^t\frac{q(t)}{\bar{\mu}\bar{c}_t^{**}}dt \tag{B39}$$

Calculate the integral of eq B30 and substitute eq B39 into eq B30:

$$\frac{m(p_i)-m(p)}{q(t)}=\frac{2p_i}{c_{ti}^*\mu_i Z_i^* G}t_{ca}^* \tag{B40}$$

Substituting eq B15 into eq 40, we obtain

$$\frac{m(p_i)-m(p)}{q(t)}=\frac{2p_i}{c_{ti}^*\mu_i Z_i G_m}t_{ca}^* \tag{B41}$$

By taking the derivative of eq B41, we obtain

$$q(t)B_{gi}=-\frac{c_{ti}^*\mu_i Z_i^* G}{2p_i}\frac{dm}{dt_{ca}^*} \tag{B42}$$

and

https://doi.org/10.1021/acsomega.2c01662
ACS Omega 2022, 7, 20927−20944

$$G_m = \frac{\pi(r_e^2 - r_w^2)h\phi_m}{B_{gi}} \tag{B43}$$

Substituting eq B43 into eq B42, we obtain

$$q(t)B_{gi} = -\frac{\pi(r_e^2 - r_w^2)h\phi_m c_{ti}^* \mu_i Z_i}{2p_i}\frac{dm}{dt_{ca}^*} \tag{B44}$$

For a radius r, we obtain

$$q_r(t)B_{gi} = -\frac{\pi(r_e^2 - r^2)h\phi_m c_{ti}^* \mu_i Z_i}{2p_i}\frac{dm}{dt_{ca}^*} \tag{B45}$$

Assuming $r_w \ll r_e$, from eqs B45 and B44, we obtain

$$q_r = q\left(1 - \frac{r^2}{r_e^2}\right) \tag{B46}$$

In the state of pseudosteady flow, considering the Darcy flow, we obtain

$$q\left(1 - \frac{r^2}{r_e^2}\right)B_g = \frac{2\pi\alpha r h k_{av}}{\mu}\frac{dp}{dr} \tag{B47}$$

Substituting eqs B17 and B26 into eq B47 and integrating eq B47, we obtain

$$q\int_{r_w}^{r}\left(1 - \frac{r^2}{r_e^2}\right)\frac{dr}{r} = \frac{\alpha\pi T_{sc}k_{av}}{p_{sc}T}h\int_{m(p_{wf})}^{m(p_r)} dm \tag{B48}$$

Assuming $r_w \ll r_e$, we obtain

$$m(p_r) = m(p_{wf}) + \frac{qp_{sc}T}{\alpha\pi T_{sc}k_{av}h}\left(\ln\left(\frac{r}{r_w}\right) - \frac{r^2}{2r_e^2}\right) \tag{B49}$$

and

$$m(p) = \frac{\int m(p_r)dV}{V} = \frac{\int_{r_w}^{r_e} m(p_r)(2\pi r h)dr}{\pi r_e^2 h} = \frac{2\int_{r_w}^{r_e} m(p_r)r dr}{r_e^2} \tag{B50}$$

Substituting eq B49 into eq B50, we obtain

$$m(p) = m(p_{wf}) + \frac{qp_{sc}T}{\alpha\pi T_{sc}k_{av}h}\left[\ln\left(\frac{r_e}{r_w}\right) - \frac{3}{4}\right] \tag{B51}$$

Define the following expression:

$$b_{pss} = \frac{p_{sc}T}{\alpha\pi T_{sc}k_{av}h}\left[\ln\left(\frac{r_e}{r_w}\right) - \frac{3}{4}\right] \tag{B52}$$

Substituting eq B52 into eq B51, we obtain

$$m(p) = m(p_{wf}) + qb_{pss} \tag{B53}$$

Substituting eq B53 into eq B40, we obtain

$$\frac{m(p_i) - m(p_{wf})}{q(t)} = \frac{2p_i}{c_{ti}^*\mu_i Z_i^* G}t_{ca}^* + b_{pss} \tag{B54}$$

Substituting eq B54 into eq B41, we obtain

$$\frac{q}{m(p_i) - m(p_{wf})} = \frac{1}{b_{pss}} - \frac{1}{b_{pss}G}\frac{m(p_i) - m(p)}{m(p_i) - m(p_{wf})}G \tag{B55}$$

AUTHOR INFORMATION

Corresponding Author

Yizhong Zhang − *Innovation Center of Unconventional Oil & Gas Resources, Yangtze University, Wuhan 434023, China;* orcid.org/0000-0002-9773-8620; Email: yizhongzhang@yangtzeu.edu.cn

Authors

Long Yang − *School of Petroleum Engineering, Yangtze University, Wuhan 434023, China;* orcid.org/0000-0002-9953-2917

Maolin Zhang − *Innovation Center of Unconventional Oil & Gas Resources, Yangtze University, Wuhan 434023, China*

Yong Liu − *Exploration and Development Research Institute of Daqing Oilfield Co. Ltd., Daqing 163453, China; Heilongjiang Provincial Key Laboratory of Reservoir Physics & Fluid Mechanics in Porous Medium, Daqing 163453, China*

Zhenqiang Bai − *Exploration and Development Research Institute of Daqing Oilfield Co. Ltd., Daqing 163453, China; Northeast Petroleum University, Daqing 163453, China*

Bin Ju − *School of Oil and Gas Engineering, Southwest Petroleum University, Chengdu 610500, China*

Complete contact information is available at: https://pubs.acs.org/10.1021/acsomega.2c01662

Author Contributions

Y.Z. and Y.L. were involved in conceptualization and methodology preparation; M.Z. was involved in supervision; Z.B. was involved in data analysis; L.Y. was involved in data collection; and B.J. was involved in documentation.

Notes

The authors declare no competing financial interest.

ACKNOWLEDGMENTS

The authors would like to acknowledge the support from the Hubei Cooperative Innovation Center of Unconventional Oil and Gas, Yangtze University and the School of Petroleum Engineering, Yangtze University. We are grateful for support from the National Natural Science Foundation of China (NSFC Grant No.: 52004032).

NOMENCLATURE

ϕ_m	free gas porosity in the matrix, fraction
ϕ_{mt}	matrix porosity, fraction
s_{mwc}	irreducible water saturation in the matrix, fraction
ρ_b	shale density, g/cm^3
ρ_{sc}	density of shale gas at the standard state, g/cm^3
ρ_s	density of adsorbed phase at formation conditions, g/cm^3
V_L	Langmuir volume, m^3/t
p_L	Langmuir pressure, MPa
p	formation pressure, MPa
G_m	free gas reserves in the matrix, m^3
B_g	gas formation volume factor, m^3/m^3
V_m	total volume of the matrix, m^3
V_f	pore volume of the fractures, m^3
ϕ_f	fracture porosity, fraction

https://doi.org/10.1021/acsomega.2c01662
ACS Omega 2022, 7, 20927−20944

G_f free gas reserves in the fractures, m^3
s_{fwc} irreducible water saturation in fractures, fraction
G_{free} free gas reserves in the matrix and fractures, m^3
G_a reserves of adsorbed gas, m^3
G_d dissolved gas reserves in kerogen, m^3
$c(p)$ methane solubility in the kerogen, m^3/m^3
V_{diff} fraction of total volume occupied by kerogen, fraction
TOC total organic carbon, %
ρ_{ko} kerogen density, g/cm^3
ϕ_a adsorbed phase porosity, fraction
ϕ_{org} organic porosity, fraction
T temperature of the reservoir, K
ΔV_a change volume of adsorbed phase, m^3
ΔV_{cm} change volume of stress sensitivity and irreducible water expansion in the matrix, m^3
c_m matrix compressibility, MPa^{-1}
c_w water compressibility, MPa^{-1}
ΔV_{cf} change volume of stress sensitivity and irreducible water expansion in the fractures, m^3
c_f fracture compressibility, MPa^{-1}
ΔV change volume of the pore, m^3
$V_E(p)$ amount of adsorbed gas in a unit mass of shale gas, m^3/t
G_p cumulative gas production, m^3.
p_{sc} pressure at the standard condition, MPa
Z_{sc} Z-factor at the standard condition, dimensionless
T_{sc} temperature at the standard condition, K
Z Z-factor at the formation pressure, dimensionless
T temperature at the reservoir, K
G original gas-in-place, m^3
r_e control radius, m
r_w well radius, m
k_{av} average permeability, μm^2
h reservoir thickness, m
V_b total volume of rock, m^3
V_p pore volume of the matrix, m^3
V_g free gas volume in the matrix, m^3
V_a adsorbed phase volume, m^3
V_{wi} irreducible water volume, m^3

Subscript

i initial state
p current state

Superscript

n current time step
$n + 1$ next time step

Constant

b_1 −0.018931
b_2 −0.85048
b_3 827.26
b_4 −635.26
α 86.4

REFERENCES

(1) Ambrose, R. J.; Hartman, R. C.; Akkutlu, I. Y. Multi-component sorbed phase considerations for shale gas-in-place calculations. In *SPE Production and Operations Symposium*, 2011, DOI: 10.2118/141416-MS.

(2) Hartman, R. C.; Ambrose, R. J.; Akkutlu, I. Y.; Clarkson, C. R. Shale Gas-in-Place Calculations Part II—Multi-component Gas Adsorption Effects. In *North American unconventional gas conference and exhibition*, 2011, DOI: 10.2118/144097-MS.

(3) Zhang, Y.; Ju, B.; Zhang, M.; Wang, C.; Zeng, F.; Hu, R.; Yang, L. The effect of salt precipitation on the petrophysical properties and the adsorption capacity of shale matrix based on the porous structure reconstruction. *Fuel* **2022**, *310*, No. 122287.

(4) Lopez, B.; Aguilera, R. Evaluation of quintuple porosity in shale petroleum reservoirs. In *SPE Eastern Regional Meeting*, 2013, DOI: 10.2118/165681-MS.

(5) Orozco, D.; Aguilera, R. A Material Balance Equation for Stress-Sensitive Shale Gas Reservoirs Considering the Contribution of Free, Adsorbed and Dissolved Gas. In *SPE/CSUR Unconventional Resources Conference*, 2015, DOI: 10.2118/175964-MS.

(6) Zhang, Y.; Yao, S.; Zhang, M.; Zhou, X.; Mei, H.; Zeng, F. Prediction of adsorption isotherms of multicomponent gas mixtures in tight porous media by the oil−gas-adsorption three-phase vacancy solution model. *Energy Fuels* **2018**, *32*, 12166−12173.

(7) Zhang, Y.; Zhang, M.; Mei, H.; Ju, B.; Shen, J.; Ge, L.; Zeng, F. Characterization of factors affecting the well deliverability of Longmaxi shale gas in the Jiaoshiba area by multivariate statistical analysis. In *AICHE Annual Conference*, 2020, 168750.

(8) Mengal, S. A.; Wattenbarger, R. A. Accounting for adsorbed gas in shale gas reservoirs. In *SPE middle east oil and gas show and conference*, 2011, DOI: 10.2118/141085-MS.

(9) Li, Q.; Li, P.; Pang, W.; Li, D.; Liang, H.; Lu, D. A new method for production data analysis in shale gas reservoirs. *J. Nat. Gas Sci. Eng.* **2018**, *56*, 368−383.

(10) King, G. R. Material-balance techniques for coal-seam and devonian shale gas reservoirs with limited water influx. *SPE Reservoir Eng.* **1993**, *8*, 67−72.

(11) Ahmed, T. H.; Centilmen, A.; Roux, B. P. A generalized material balance equation for coalbed methane reservoirs. In *SPE annual technical conference and exhibition*, 2006, DOI: 10.2118/102638-MS.

(12) Firanda, E. The development of material balance equations for coalbed methane reservoirs. In *SPE Asia Pacific Oil and Gas Conference and Exhibition*, 2011, DOI: 10.2118/145382-MS.

(13) Penuela, G.; Ordonez, A.; Bejarano, A. A generalized material balance equation for coal seam gas reservoirs. In *SPE Annual Technical Conference and Exhibition*, 1998, DOI: 10.2118/49225-MS.

(14) Moghadam, S.; Jeje, O.; Mattar, L. Advanced gas material balance in simplified format. *J. Can. Pet. Technol.* **2011**, *50*, 90.

(15) Mattar, L.; McNeil, R. The flowing gas material balance. *J. Can. Pet. Technol.* **1998**, *37*, No. PETSOC-98-02-06.

(16) Anderson, D. M.; Mattar, L. An improved pseudo-time for gas reservoirs with significant transient flow. *J. Can. Pet. Technol.* **2007**, *46*, No. PETSOC-07-07-05.

(17) Clarkson, C. R.; Bustin, R. M.; Seidle, J. P. Production-data analysis of single-phase (gas) coalbed-methane wells. *SPE Reservoir Eval. Eng.* **2007**, *10*, 312−331.

(18) Ambrose, R. J.; Hartman, R. C.; Diaz Campos, M.; Akkutlu, I. Y.; Sondergeld, C. New pore-scale considerations for shale gas in place calculations. *SPE unconventional gas conference*, 2010, DOI: 10.2118/131772-MS.

(19) Wei, M.; Duan, Y.; Dong, M.; Fang, Q. Blasingame decline type curves with material balance pseudo-time modified for multi-fractured horizontal wells in shale gas reservoirs. *J. Nat. Gas Sci. Eng.* **2016**, *31*, 340−350.

(20) Zhang, Y.; He, Z.; Jiang, S.; Lu, S.; Xiao, D.; Chen, G.; Li, Y. Fracture types in the lower Cambrian shale and their effect on shale gas accumulation, Upper Yangtze. *Mar. Pet. Geol.* **2019**, *99*, 282−291.

(21) Dejam, M.; Hassanzadeh, H.; Chen, Z. Semi-analytical solution for pressure transient analysis of a hydraulically fractured vertical well in a bounded dual-porosity reservoir. *J. Hydrol.* **2018**, *565*, 289−301.

(22) Zhang, T.; Li, Z.; Adenutsi, C. D.; Lai, F. A new model for calculating permeability of natural fractures in dual-porosity reservoir. *Adv. Geo-Energy Res.* **2017**, *1*, 86−92.

(23) Connell, L. D. A new interpretation of the response of coal permeability to changes in pore pressure, stress and matrix shrinkage. *Int. J. Coal Geol.* **2016**, *162*, 169−182.

(24) Liu, T.; Tang, H.; Liu, P.; Lin, W.; Su, G. Material balance equation and reserves calculation method for fractured closed shale gas reservoirs. *Nat. Gas Explor. Dev.* **2011**, *34*, 28−30.

https://doi.org/10.1021/acsomega.2c01662
ACS Omega 2022, 7, 20927−20944

(25) Wang, D.; Guo, P.; Chen, H.; Fu, W.; Wang, Z.; Ding, H. Deduction of material balance equation and reserves calculation for new adsorbed gas reservoirs. *Lithol. Reservoirs* **2012**, *24*, 83−86.
(26) Yang, L.; Mei, H.; Zhang, M.; Yuan, E. Calculation method of shale gas reservoir reserves considering dissolved gas in kerogen. *Xinjiang Pet. Geol.* **2016**, *05*.
(27) Orozco, D.; Aguilera, R. A material-balance equation for stress-sensitive shale-gas-condensate reservoirs. *SPE Reservoir Eval. Eng.* **2017**, *20*, 197−214.
(28) He, L.; Mei, H.; Hu, X.; Dejam, M.; Kou, Z.; Zhang, M. Advanced flowing material balance to determine original gas in place of shale gas considering adsorption hysteresis. *SPE Reservoir Eval. Eng.* **2019**, *22*, 1282−1292.
(29) Meng, Y.; Li, M.; Xiong, X.; Liu, J.; Zhang, J.; Hua, J.; Zhang, Y. Material balance equation of shale gas reservoir considering stress sensitivity and matrix shrinkage. *Arabian .o Geosci.* **2020**, *13*, 1−9.
(30) Williams-Kovacs, J. D.; Clarkson, C. R.; Nobakht, M. Impact of material balance equation selection on rate-transient analysis of shale gas. In *SPE Annual Technical Conference and Exhibition*, 2012, DOI: 10.2118/158041-MS.
(31) Dejam, M. Advective-diffusive-reactive solute transport due to non-Newtonian fluid flows in a fracture surrounded by a tight porous medium. *Int. J. Heat Mass Transfer* **2019**, *128*, 1307−1321.
(32) Langmuir, I. The adsorption of gases on plane surfaces of glass, mica and platinum. *J. Am. Chem. Soc.* **1918**, *40*, 1361−1403.
(33) Mehrotra, A. K.; Svrcek, W. Y. Correlations for properties of bitumen saturated with CO2, CH4 and N2, and experiments with combustion gas mixtures. *J. Can. Pet. Technol.* **1982**, *21*, No. PETSOC-82-06-05.
(34) Fetkovich, M. J. Decline curve analysis using type curves. In *Fall Meeting of the Society of Petroleum Engineers of AIME*, 1973, DOI: 10.2118/4629-MS.

https://doi.org/10.1021/acsomega.2c01662
ACS Omega 2022, 7, 20927−20944